

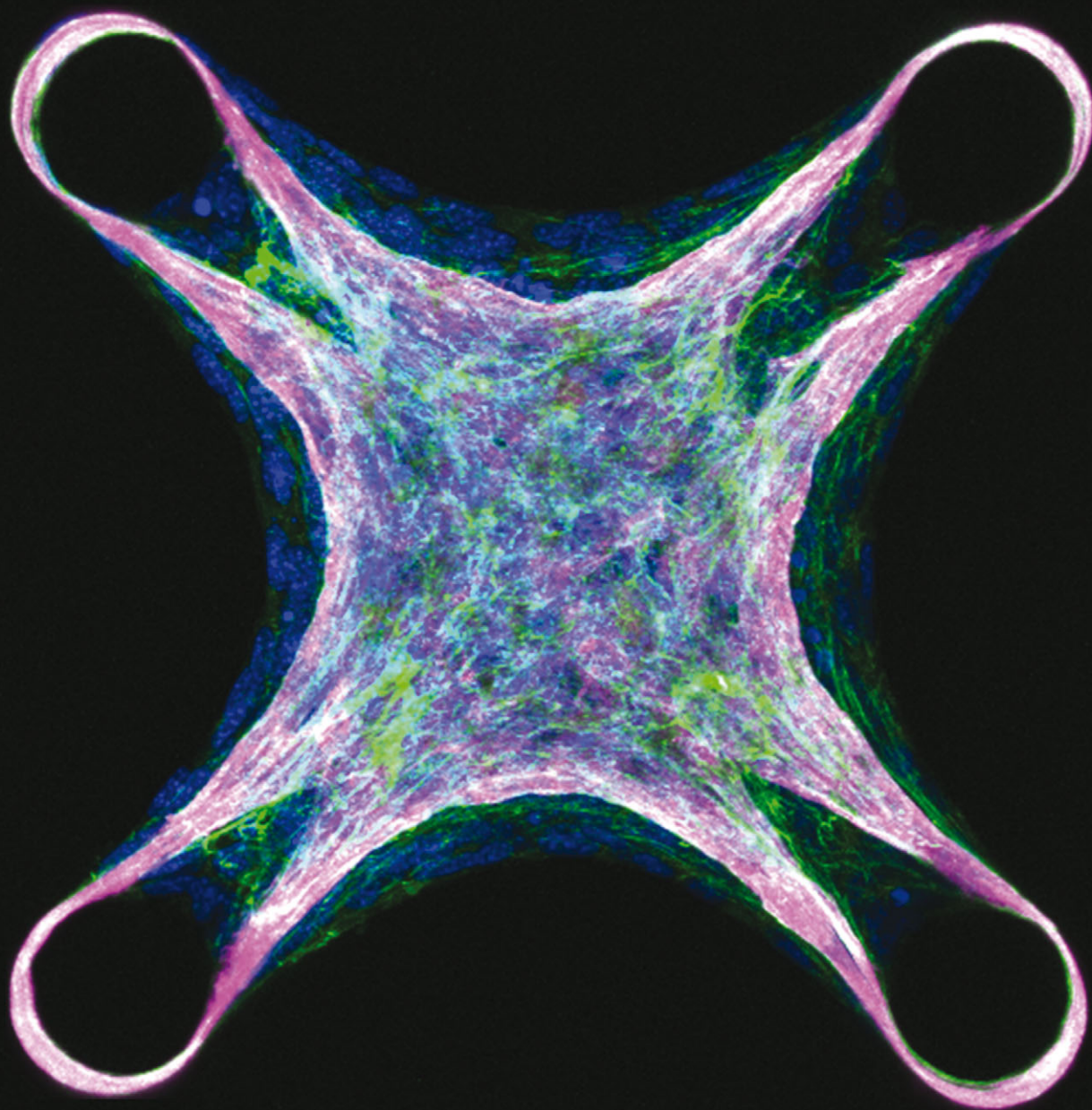
Indexed in
MEDLINE!

Integrative Biology

Quantitative biosciences from nano to macro

www.rsc.org/ibiology

Volume 4 | Number 10 | October 2012 | Pages 1145–1312



Downloaded on 16 October 2012
Published on 15 August 2012 on http://pubs.rsc.org | doi:10.1039/C2IB20059G

ISSN 1757-9694

RSC Publishing

PAPER

Christopher S. Chen, Viola Vogel *et al.*
Force-induced fibronectin assembly and matrix remodeling in a
3D microtissue model of tissue morphogenesis



1757-9694(2012)4:9;1-M

Cite this: *Integr. Biol.*, 2012, 4, 1164–1174

www.rsc.org/ibiology

PAPER

Force-induced fibronectin assembly and matrix remodeling in a 3D microtissue model of tissue morphogenesis†

Wesley R. Legant,^a Christopher S. Chen^{*a} and Viola Vogel^{*b}

Received 15th March 2012, Accepted 12th August 2012

DOI: 10.1039/c2ib20059g

Encapsulations of cells in type-I collagen matrices are widely used three-dimensional (3D) *in vitro* models of wound healing and tissue morphogenesis and are common constructs for drug delivery and for *in vivo* implantation. As cells remodel the exogenous collagen scaffold, they also assemble a dense fibronectin (Fn) matrix that aids in tissue compaction; however, the spatio-temporal (re)organization of Fn and collagen in this setting has yet to be quantitatively investigated. Here, we utilized microfabricated tissue gauges (μ TUGs) to guide the contraction of microscale encapsulations of fibroblasts within collagen gels. We combined this system with a Foerster Radius Energy Transfer (FRET) labeled biosensor of Fn conformation to probe the organization, conformation and remodeling of both the exogenous collagen and the cell-assembled Fn matrices. We show that within hours, compact Fn from culture media adsorbed to the collagen scaffold. Over the course of tissue remodeling, this Fn-coated collagen scaffold was compacted into a thin, sparsely populated core around which cells assembled a dense fibrillar Fn shell that was rich in both cell and plasma derived Fn. This resulted in two separate Fn populations with different conformations (compact/adsorbed and extended/fibrillar) in microtissues. Cell contractility and microtissue geometry cooperated to remodel these two populations, resulting in spatial gradients in Fn conformation. Together, these results highlight an important spatio-temporal interplay between two prominent extracellular matrix (ECM) molecules (Fn and collagen) and cellular traction forces, and will have implications for future studies of the force-mediated remodeling events that occur within collagen scaffolds either in 3D *in vitro* models or within surgical implants *in vivo*.

Introduction

Three-dimensional (3D) encapsulations of cells in type-I collagen have served as *in vitro* models of tissue morphogenesis and

wound healing for nearly thirty years¹ and more recently as a strategy for drug delivery, and for *in vivo* implantation.² Cells within these matrices exert contractile forces on the surrounding matrix fibers, resulting in a dramatic reorganization of the extracellular environment and the self-assembly of a coherent tissue-like structure. Concurrent with the modification of the exogenous collagen scaffold, cells also assemble a dense meshwork of additional extracellular matrices (ECMs) including fibronectin (Fn)³ and tenascins⁴ as well as other proteins.⁵ During morphogenetic events *in vivo*, a Fn matrix serves as a provisional template that directs the assembly of more permanent collagen fibers.^{6,7} However, it is not clear to what extent the inverse is true,

^a Department of Bioengineering, University of Pennsylvania, 210 S, 33rd Street, Philadelphia, PA 19104, USA.

E-mail: chrischen@seas.upenn.edu

^b Department of Health Sciences and Technology, Laboratory of Applied Mechanobiology, Wolfgang-Pauli-Strasse 10, HCI F 443 ETH Zurich, CH-8093 Zurich, Switzerland.

E-mail: viola.vogel@hest.ethz.ch

† Electronic supplementary information (ESI) available: See DOI: 10.1039/c2ib20059g

Insight, innovation, integration

The remodeling of an extracellular matrix (ECM) is essential for development, wound healing and tissue homeostasis. Despite the central role of the ECM in these processes, it is not known how cell generated forces, tissue geometry and soluble enzymes coordinate to spatially pattern the ECM within tissues. Here, we combine microfabricated arrays of collagen based microtissues with a Foerster Radius Energy Transfer (FRET)

based biosensor of fibronectin conformation to spatially map the relationship between fibronectin conformation/assembly, collagen remodeling and tissue geometry in three dimensions. Our data reveal the presence of two separate populations of Fn (compact/collagen adsorbed and extended/fibrillar) that become spatially patterned during collagen compaction and are differentially remodeled by cells.

namely, how or if an exogenous collagen scaffold can direct the formation of a cell-assembled Fn matrix.

Given that the molecular conformation of Fn and indeed the physical assembly of a fibrillar Fn matrix are modulated by the same cell-generated forces that drive the reorganization of the collagen scaffold,^{8–11} it seems likely that modifications to the structure of a provisional Fn matrix would occur concurrently with collagen compaction. On two-dimensional (2D) surfaces, a mechanically extended conformation of Fn has been shown to impact matrix assembly¹² and the binding of proteins and bacterial adhesins.^{13,14} Understanding to what extent Fn is sensitive to mechanical forces when it is assembled within a composite 3D tissue in which other load bearing ECM proteins are present will be critical for translating insight from 2D studies into the more complex remodeling events that occur in 3D and *in vivo*.

A key limitation to these types of investigations has been that bulk encapsulations of cells in collagen matrices are typically millimeters to centimeters in scale.^{1,2} The optics of such large structures and the massive movements occurring from gel compaction preclude the application of traditional high-resolution fluorescence microscopy. Furthermore, cells within such gels will experience heterogeneous mechanical and soluble conditions throughout the depth of the construct. *In situ* observation of Fn conformation has recently become feasible by utilizing a Foerster Radius Energy Transfer (FRET) labeled biosensor of Fn conformation,^{10,15} but previous applications of this tool have been limited to 2D cultures or very thin (<20 microns) cell derived matrices.¹² To address the optical limitations of centimeter-scale constructs, we have recently established micro-electro-mechanical (MEMS) based microfabricated tissue gauges (μ TUGs) in which one can observe compaction of nanoliter-scale 3D microtissues consisting of hundreds of cells encapsulated in type-I collagen gels.^{16,17}

Here, we combine μ TUGs with a FRET biosensor of Fn conformation to probe the organization, conformation and remodeling of both the exogenous collagen scaffold and the cell-assembled Fn matrices during force-mediated tissue condensation. By incorporating this biosensor at different stages of tissue remodeling, and under different tissue geometries, we observe the presence and spatial localization of two separate Fn populations with different conformations (compact/collagen-adsorbed and extended/fibrillar) that may have different downstream signaling properties.^{10,12–14} By tethering microtissues to flexible cantilevers, we report the forces generated during collagen remodeling and confirm that increases in tissue stress are accompanied by the assembly of a progressively unfolded fibrillar Fn matrix. Together, these results highlight how Fn is organized during collagen compaction and will have important implications for future studies of the remodeling events that occur within collagen scaffolds either in 3D *in vitro* models or within surgical implants *in vivo*.

Results

Utilization of micropatterned tissue gauges to generate collagen based microtissues

In order to micropattern encapsulations of cells in collagen matrices, we used SU-8 photolithography to generate arrays of wells (400 μ m \times 400 μ m \times 110 μ m deep) on a silicon wafer

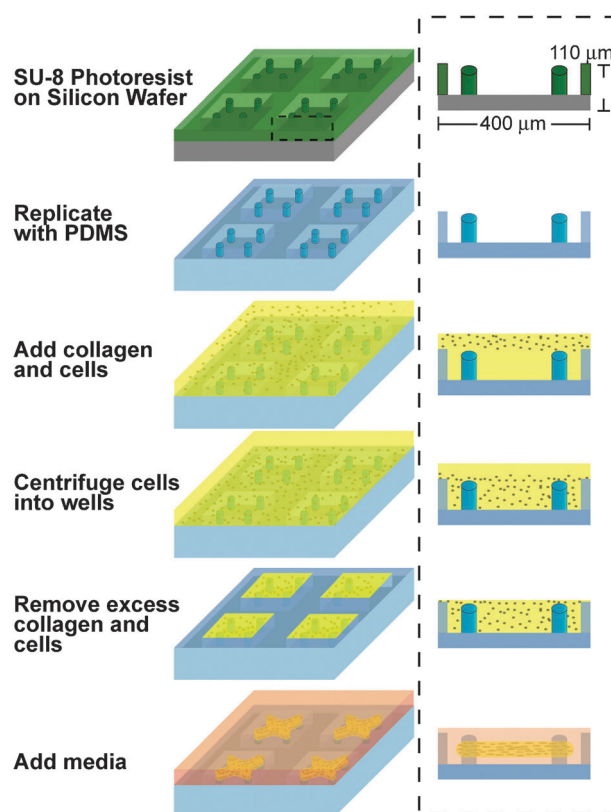


Fig. 1 Fabrication and seeding of microfabricated tissue gauge (μ TUG) molds. Process flow diagram for the creation of μ TUG arrays. After replicating the rigid photoresist structures with a PDMS elastomer, the mold is immersed within a prepolymer solution of cells and type-I collagen. The entire assembly is then centrifuged to drive the cells into the templates. Excess solution is removed and the matrix is polymerized (by increasing the temperature to 37 °C) prior to adding media.

(Fig. 1). Within each well, we incorporated raised cantilevers that served to constrain the final tissue geometry. After replicating the rigid photoresist structures with a polydimethylsiloxane (PDMS) elastomer, we immersed the mold within a prepolymer solution of NIH 3T3 cells and type-I collagen. The entire assembly was centrifuged to drive the cells into the templates before removing excess solution and polymerizing the matrix. Within hours, the encapsulated cells began to remodel the adjacent matrix fibers. The collective matrix remodeling by all cells within the construct condensed the tissue into a coherent band that became anchored to the cantilevers. Within this system, we also observed that as cells remodel the collagen gel, they simultaneously assembled a dense Fn matrix. It has previously been shown that the assembly of Fn fibers is regulated by cell traction forces both *in vitro*^{9,11} and *in vivo*⁸ and can be modulated by the amount of mechanical stress within microtissues;¹⁷ however, the spatio-temporal relationship between the Fn matrix and the collagen scaffold during compaction has not been studied in detail. As the chemical and mechanical microenvironment within which Fn is assembled can impact its conformation^{18,19} and therefore the accessibility of cryptic binding sites, we sought to precisely map the spatial distributions of Fn and collagen within the microtissue system.

Cells condense the collagen matrix into a densely aligned core around which they form a highly cellularized shell containing fibrillar fibronectin

Within 24 hours, cells contract the collagen scaffold into a coherent tissue that was tethered around the cantilevers. Over 72 hours, the collagen scaffold was compacted into a dense core from which the cells had mostly receded into a highly cellularized peripheral shell (Fig. 2, Fig. S1 and Movies S1–S5, ESI†). The use of primary antibodies specific for rat-tail collagen ensured that we only examined the localization of the original collagen scaffold and not collagen assembled *de novo* by the constituent cells. DAPI staining was uniform throughout the horizontal plane of the tissue; however, 3D density mapping of tissue cross sections confirmed the presence of a cellularized shell about a sparsely populated collagen scaffold with the highest cell density on the top surface. Within hours of encapsulation, plasma Fn from the culture media adsorbed to the collagen scaffold and the distributions of the two matrices were nearly identical after 24 hours (Fig. 2a and Fig. S1a, ESI†); however, over the next

several days, the matrices formed distinct patterns (Fig. 2b, c and Fig. S1b, c, ESI†). The collagen was compacted and aligned within the interior of the tissue, with highest densities at the perimeter of this core. Fn in contrast was assembled in concentric shells around the collagen core and Fn fiber density was up-regulated and aligned in regions of the tissue that have previously been suggested to be under high mechanical tension (Fig. S2, ESI†).¹⁷ Acute (2 hour incubation just prior to fixation) treatment with blebbistatin did not dramatically alter the distributions of plasma Fn, collagen or DAPI, but did cause a relaxation of the tissue as observed by a decrease in the radius of tissue curvature between the boundaries (Fig. 2d and Fig. S1d, ESI†).

Interestingly, although the amount of fibrillar Fn in the microtissues increased over time, the intensity of the plasma Fn fluorescent signal decreased, possibly due to a combination of a gradual dilution with endogenous cell-secreted Fn molecules in fibrils and protease mediated degradation of plasma Fn. To more rigorously test this hypothesis, we performed dual labeling of both fluorescently labeled plasma Fn, and anti-EDA Fn (a splice isoform specific to cell-derived Fn). After 72 hours, both cellular and plasma Fn were largely colocalized in the peripheral fibrillar matrix; however, only plasma Fn was localized to the collagen scaffold (Fig. S3 and Movies S4, S5, ESI†). These data indicate that the collagen-adsorbed Fn is predominantly from plasma whereas the fibrillar matrix assembled at later time points consists of both cell-derived and plasma Fn.

Plasma fibronectin is progressively assembled into more mechanically extended fibers during the remodeling of a collagen scaffold

As the outside-in cell signaling mediated by Fn is not only dependent on its presence or absence, but also on its physical and conformational presentation,²⁰ we next sought to determine whether the changes in Fn distribution that occur during tissue remodeling also correlate with changes in the conformation of the Fn molecules presented to cells. We incubated 4-post microtissues with a FRET based biosensor of Fn conformation (Fibronectin–Donor/Acceptor labeled, Fn–DA) and fixed after 24, 48 or 72 hours of remodeling. By acquiring confocal sections, the FRET signal can be used to map 3D Fn conformation within the tissue. It should be noted, however, that these data only represent the conformation of the exogenous plasma Fn molecules, and not the contribution from the endogenous cell-derived Fn. Further, the Fn–DA probe reports the average distance between donor and acceptor fluorophores on the Fn molecule and can thus be used to report conformational changes; however, because the acceptors are labeled on the FnIII₇ and FnIII₁₅ modules, we are only probing structural changes within ~12 nm of these regions (yellow circle in Fig. 3a). Finally, only a small fraction (10%) of the exogenous plasma Fn molecules are labeled with fluorophores to avoid the possibility of intermolecular FRET,¹⁰ thus assuring that the FRET signal within fibrils reports the molecular conformation, and will not be affected by changes in the concentration of plasma Fn in fibrils (*e.g.* as it gradually becomes diluted with endogenous cell-derived Fn).

We report the FRET ratio as the acceptor intensity (I_a) divided by the donor intensity (I_d) after correction for spectral

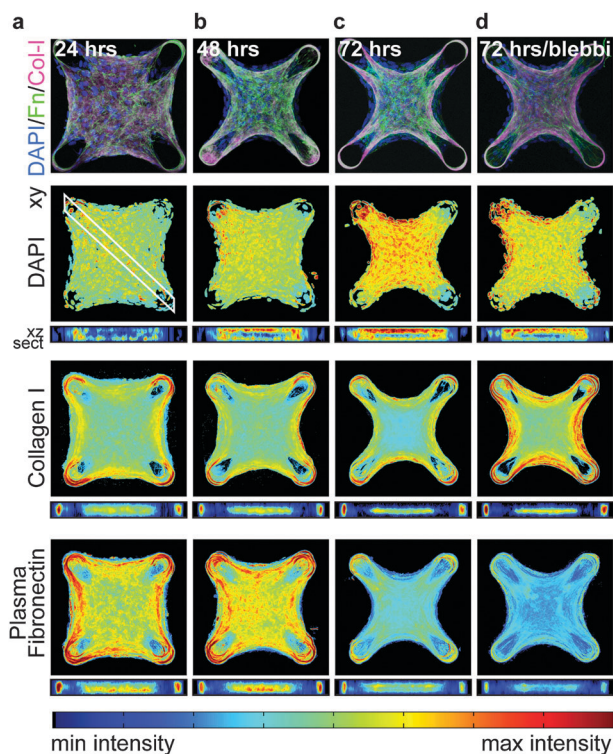


Fig. 2 3D averaged density maps of ECM protein in microtissues. (a–d) Immunofluorescent images showing DAPI, collagen I and plasma Fn within microtissues fixed after 24, 48 and 72 hours of remodeling, or after 72 hours of remodeling with acute (2 hours prior to fixing) incubation with 50 μ M blebbistatin. Density maps represent the DNA or protein density, respectively, at a given location averaged over the axis orthogonal to the image plane. In order to register images between tissues of different thickness, cross-sections (xz sect.) are plotted from the uppermost to the lower most surface of the tissues (*i.e.* normalized by tissue thickness). All density maps are the average of 10 individual microtissues from each condition. Color scales are normalized to depict the min and max values for each stain. Thus, the intensities measured at different time points for the same stain are comparable, but the intensities of different protein stains are not.

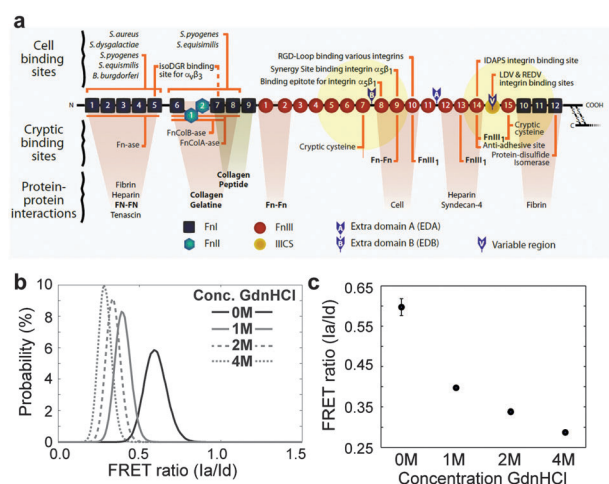


Fig. 3 Fn structure and Fn–DA FRET labeling. (a) Cartoon of a Fn monomer depicting multiple cell and ECM binding sites (adapted from Vogel, *Annu. Rev.*, 2006). Yellow sphere represents the 12 nm radius of potential energy transfer to acceptor labeled cysteines (twice the Förster radius). Donors are randomly labeled at amines at an average of 7 donors and 4 acceptors per molecule. (b) Probability density functions (PDFs) of the FRET ratios from Fn–DA in solution with increasing concentrations of the denaturant GdnHCl. (c) Mean values for the histograms depicted in b. Fn begins to lose its secondary structure at or below 1 M GdnHCl ($I_a/I_d = 0.40$) and is completely denatured at 4 M GdnHCl ($I_a/I_d = 0.29$). (b, c) The average (\pm SD) of 5 fields of view under each condition.

bleed-through and acceptor cross-talk as detailed in Methods. In order to correlate the FRET ratio seen in microtissues to structural changes in the Fn molecule, we calibrated the FRET ratio to soluble Fn–DA in known concentrations of the denaturant guanidine hydrochloride (GdnHCl) (Fig. 3b and c). Previous work has demonstrated that the transition from compact Fn to an extended molecule correlates with the drop of the FRET signal seen for Fn–DA in solution between 0 M and 1 M GdnHCl. Moreover, Fn in solution begins to lose its secondary structure at concentrations of denaturant GdnHCl approaching 1 M ($I_a/I_d = 0.40$), with complete denaturation at 4 M GdnHCl ($I_a/I_d = 0.29$).¹⁰

We found that after 24 hours, the Fn–DA within microtissues existed predominantly in a compact conformation, but that there was a significant drop in the median FRET ratio of Fn–DA as the tissue remodeled from 0.62 to 0.57 and 0.51, after 24, 48 and 72 hours, respectively (Fig. 4a, b and Table S1, ESI†). Acute treatment with blebbistatin after 72 hours revealed that approximately 40 percent of the decrease in FRET was due to active cellular contractility whereas the remaining 60 percent was unaffected. By simultaneously imaging the FRET signal and the immunofluorescence staining of the collagen scaffold, we separated the Fn–DA population within microtissues into collagen-colocalized Fn–DA and non-collagen-colocalized Fn–DA to determine if these two populations might respond differently. At each time point, we found that collagen-colocalized Fn–DA was more compact than non-collagen-colocalized Fn–DA, and that both populations appeared to be progressively unfolded over time (Fig. 4c and d) to within our measurement resolution ($0.621 \times 0.621 \times 2.0 \mu\text{m}$).

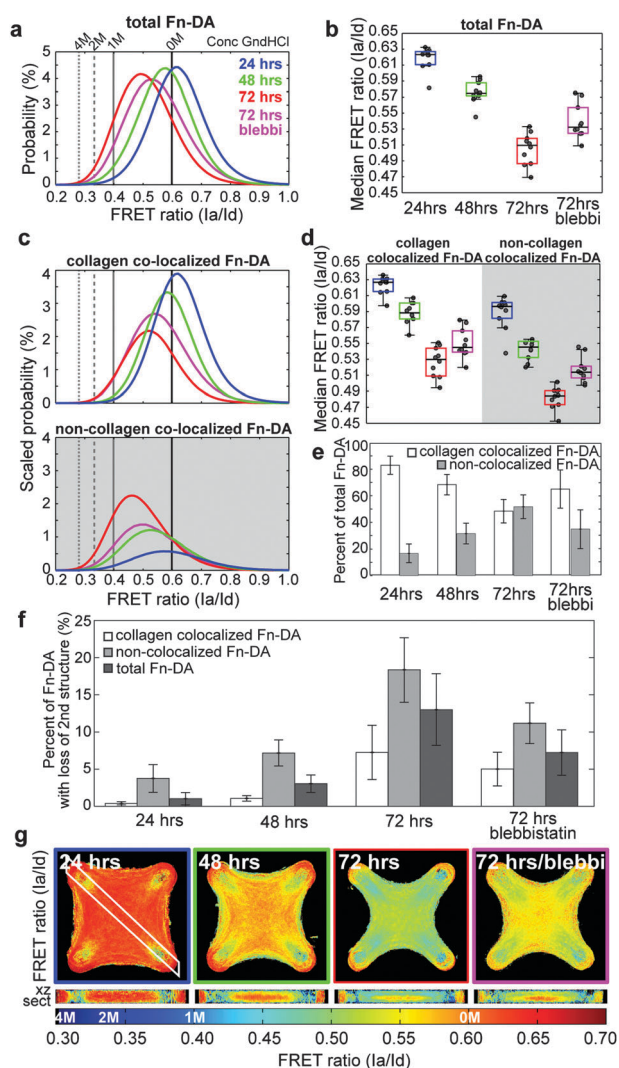


Fig. 4 FRET measurement of Fn conformation in microtissues. (a) PDFs of total Fn–DA measured in microtissues fixed after 24, 48 or 72 hours of remodeling, or after 72 hours of remodeling with acute (2 hours prior to fixing) incubation with 50 μM blebbistatin. Corresponding values from Fn–DA in solutions of 0 M, 1 M, 2 M and 4 M GdnHCl denaturant are indicated. (b) Box and whiskers plot of the median FRET values within microtissues depicted in a. (c) Scaled PDFs showing separate populations of collagen-colocalized Fn–DA and non-collagen-colocalized Fn–DA. PDFs are scaled such that the areas under each curve equal the percent of either collagen-colocalized Fn–DA or non-collagen-colocalized Fn–DA at each time point. (d) Box and whiskers plot of the median FRET values within microtissues depicted in c showing either collagen-colocalized Fn–DA or non-collagen-colocalized Fn–DA. (e) Percent of Fn–DA within microtissues fixed at each time point that is either colocalized with collagen, or non-collagen-colocalized. (f) Percent of either collagen-colocalized, non-collagen-colocalized, or total Fn–DA present in microtissues with a loss in secondary structure (FRET ratios below that of Fn in 1 M GdnHCl). (g) Average density maps of the FRET ratios (I_a/I_d) within microtissues from a–f. Corresponding denaturation points are indicated on the colorbar. All data and images were computed from 10 microtissues within each condition. Data in a–f were computed from the raw experimental data and not from the density maps. Data from a and c are the compiled PDFs for all microtissues within a given condition. Data from e are mean values \pm SD.

Interestingly, there was a gradual shift from predominantly collagen-colocalized Fn-DA (83% colocalized *vs.* 17% non-colocalized after 24 hours) to nearly equal amounts of colocalized and non-colocalized Fn-DA after 72 hours (48% colocalized *vs.* 52% non-colocalized) (Fig. 4e). These two factors combined result in an increase in the amount of total Fn-DA presented to cells that has a loss in secondary structure (as based on the GdnHCL data) from 1%, 3% to 13% after 24, 48 and 72 hours, respectively (Fig. 4f).

Cellular contractility and microtissue geometry direct 3D gradients in fibronectin conformation

Average FRET values within a microtissue only represent a limited view of the story. In contrast to soluble factors which are capable of diffusing throughout the tissue, conformational changes in the structure of Fn will only signal to cells if they are capable of physically interacting with the molecule (*i.e.* cells within tens of microns of a given binding site). We thus sought to determine whether the gradients in Fn concentration we observed previously also correlated with gradients in the conformation of the Fn-DA molecules by taking average density maps of the FRET signal within the microtissues. We found that after 24 hours, Fn-DA appeared to primarily be adsorbed to the collagen gel with no clear conformational gradients present in the tissue. However over the course of remodeling, Fn-DA became progressively fibrillar and increasingly strained with clear gradients emerging in both the horizontal and vertical tissue planes (Fig. 4g and Movies S1–S3, ESI†). The highest FRET ratios (compact Fn-DA) occurred at the core of the constructs, in regions where dense collagen staining was also observed. In contrast, the lowest FRET ratios (mechanically stretched Fn-DA) occurred predominantly near the surface of the microtissue, in regions that were spatially separated from the collagen scaffold. Acute treatment with blebbistatin did not shift the spatial FRET distributions, but rather increased the FRET signal within both the core and periphery of the microtissue.

Within this geometry, we observed gradients in Fn-DA conformation that appeared to be correlated with regions of the tissue that would be subjected to high mechanical tension. Moreover, previous studies have shown that the presence of Fn can dramatically increase the ability of cells to compact a collagen scaffold.²¹ We therefore wanted to measure whether increases in tissue stress occurred concurrently with the assembly of a fibrillar Fn matrix. However, as the cantilevers in the 4-post configuration are rigid, we could not directly measure the tissue stress. To address this, we next cultured microtissues within PDMS molds that contained 2 flexible cantilevers (400 μm \times 800 μm \times 150 μm deep) (Fig. 5a and Movies S6, S7, ESI†). We utilized multilayer SU-8 photolithography to generate wide caps at the tips of the flexible cantilevers¹⁷ that serve to anchor the tissue even when the cantilever becomes highly deflected. By displacing the cantilever tip with a MEMS strain sensor, we determined the cantilever spring constant to be $148 \pm 35 \text{ nN } \mu\text{m}^{-1}$ which was linear over the range of displacements tested (Fig. 5b and c). This spring constant was then used to relate cantilever bending to microtissue force.

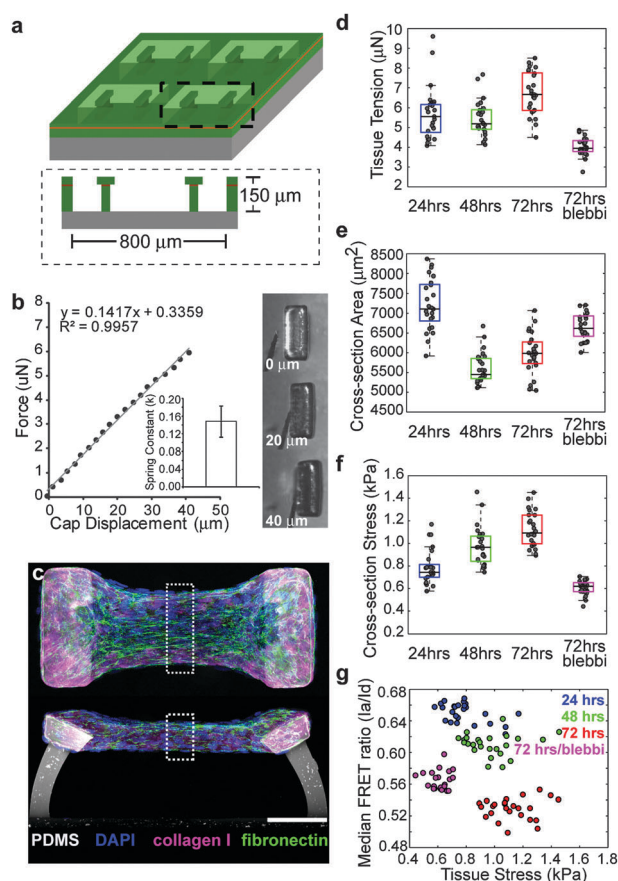


Fig. 5 Increases in tissue stress occur concurrently with the assembly of a progressively unfolded fibrillar Fn matrix. (a) Schematic of 2 post μTUG molds generated from multilayer SU-8 photolithography. (b) Calibration of cantilever spring constants and corresponding transmitted light images of cap deflection. A representative plot of force *vs.* cap displacement is shown. Inset: calculated spring constant ($k = 148 \pm 35 \text{ nN } \mu\text{m}^{-1}$ (SD) for $n = 15$ measurements, 5 cantilevers each across 3 substrates). (c) Representative top down and cross-section views for microtissues showing Fn (green), collagen (pink) and DAPI (blue) after 48 hours of remodeling. Dashed boxes indicate regions for calculation of cross-sectional area, cross-sectional stress and Fn-DA FRET. Scale bar = 100 μm . (d) Box and whiskers plot of tissue tension for 2-post microtissues fixed after 24, 48 and 72 hours of remodeling, or after 72 hours of remodeling with acute (2 hours prior to fixing) incubation with 50 μM blebbistatin. (e) Box and whiskers plot of cross-sectional area for tissues under the same conditions as d. (f) Box and whiskers plot of cross-sectional stress for tissues under the same conditions as d. (g) Scatter plot for the median FRET ratio (I_a/I_d) *vs.* cross-sectional stress for tissues under the same conditions as d. (d–g) Computed from 25 individual microtissues under each condition.

Increases in microtissue stress occur concurrently with the peripheral assembly of a progressively unfolded fibrillar fibronectin matrix

In microtissues tethered to two flexible cantilevers, we found that tissue tension increased during the first 24 hours and then leveled off at approximately 5.5 μN before a moderate increase in force between 48 and 72 hours to 6.7 μN (Fig. 5d and Table S2, ESI†). The cross-sectional area of the elongated microtissues decreased dramatically between 24 and 48 hours, but

then increased between 48 and 72 hours due to increased cell proliferation at the periphery of the tissue (Fig. 5e and Table S2, ESI†). As a result, median cross-sectional tissue stress increased progressively from 740 to 970 to 1090 Pa after 24, 48 and 72 hours, respectively (Fig. 5f and Table S2, ESI†). Concurrent with these increases in stress, we found that the median FRET ratios of Fn–DA within these tissues decreased from 0.66 to 0.61 to 0.53 at each of these time points (Fig. 5g, Fig. S4 and Table S2, ESI†). Similar to the 4 post configuration, a portion of the Fn remodeling was actively mediated by cell contractile forces. Acute (2 hour incubation just prior to fixation) blebbistatin treatment after 72 hours of remodeling led to a dramatic decrease in tissue stress to 620 Pa, but only a partial restoration of FRET signals at approximately 0.56. Thus the increased tissue stress that occurs during the remodeling of a collagen scaffold correlates with a progressively stretched and unfolded Fn matrix assembled at the periphery. However, we did not observe a relationship between tissue stress and Fn–DA FRET *within* each time point despite nearly a 2-fold variation in stress between tissues, thus it seems unlikely that these two parameters are directly related (*i.e.* that tissue stress is transmitted directly to Fn fiber strains or *vice versa*). In microtissues, it is possible that most of the tissue stress may be transmitted not through the Fn matrix, but instead through the exogenous collagen scaffold or through direct transmission *via* the actin cytoskeleton and cell–cell junctions.

Fn–DA that is initially adsorbed to the collagen scaffold is not incorporated into the fibrillar fibronectin matrix, nor is it progressively stretched by cells

In the previous section, we demonstrated that both collagen-colocalized Fn–DA and non-collagen-colocalized Fn–DA molecules became progressively stretched as the microtissue remodeled. However, because Fn–DA was continually present in the culture medium throughout the experiment, it was not clear whether the decrease in FRET observed for these two populations was due to the gradual stretching of the original Fn–DA molecules, or due to the adsorption/assembly of new Fn–DA molecules in a more unfolded state. To test the relative roles of these processes, we incubated microtissues tethered to 4 posts with pulses of labeled Fn–DA from 0–24 hours, 24–48 hours, or 48–72 hours before fixing. This experiment only labels Fn present in the system during a given window of time. We found that Fn–DA present during the first 24 hours of remodeling existed predominantly in a compact conformation and was not progressively strained by cells (Fig. 6a and Table S3, ESI†). Microtissues incubated with Fn–DA for the first 24 hours of remodeling displayed the same FRET ratios whether they were fixed after 24 hours, or whether the Fn–DA was replaced with unlabeled Fn and the labeled matrix was allowed to be remodeled for an additional 48 hours. This lack of molecular extension occurred for both collagen-colocalized and non-collagen-colocalized populations (Fig. 6b and Table S3, ESI†). In contrast, both collagen-colocalized and non-collagen-colocalized Fn–DA present at the later stages of tissue remodeling (48–72 hours) displayed dramatically lower FRET ratios despite only being remodeled by cells for a period of 24 hours (Fig. 6a, b and Table S3, ESI†).

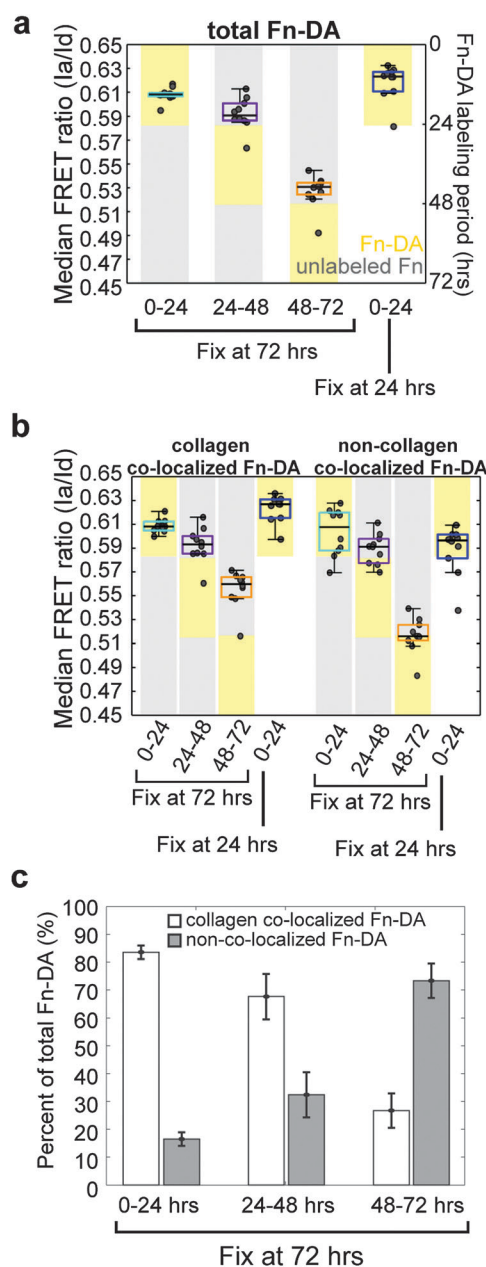


Fig. 6 Fn–DA pulse-chase experiments and colocalization analysis for 4-post microtissues. Fn–DA (yellow boxes) or unlabeled Fn (grey boxes) was present in culture for specified windows during tissue remodeling. Microtissues were then fixed at the indicated times and FRET signals recorded. (a) Box and whiskers plot of the median FRET ratios (I_a/I_0) for microtissues fixed after 72 hours in which Fn–DA was present between either 0–24, 24–48, or 48–72 hours or for microtissues fixed immediately after the first 24 hours of remodeling. (b) Box and whiskers plot of the median FRET ratios (I_a/I_0) showing either collagen-colocalized Fn–DA or non-collagen-colocalized Fn–DA for the same conditions as a. (c) Percent of Fn–DA within microtissues assembled at the indicated increments that is either colocalized with collagen or non-colocalized with collagen. Data from a–c are from 10 microtissues in each condition. Data from b are mean values \pm SD.

We next examined the spatio-temporal organization of both the collagen scaffold and Fn–DA molecules incorporated during

given stages of microtissue remodeling. When microtissues were fixed after 24 hours, we found that 80% of the Fn-DA was co-localized with the collagen scaffold (Fig. 4e). If, instead of fixing the sample after 24 hours, we replaced the Fn-DA with unlabeled Fn and allowed the microtissue to continue remodeling for an additional 48 hours, we found that nearly all labeled Fn-DA was still highly co-localized (85%) with the collagen scaffold (Fig. 6c). Moreover, the non-collagen-colocalized Fn-DA appeared immediately adjacent to the collagen scaffold (Movie S8, ESI†). Thus, even after 72 hours, the Fn-DA molecules incorporated into the construct during the early stages of remodeling exist predominantly in a compact conformation that is either bound to or in very close proximity to the collagen scaffold. This interaction appears to stabilize the Fn molecules such that they are not progressively stretched by cells nor incorporated into fibrils as the tissue remodels. In contrast, Fn-DA present between 48 and 72 hours was predominantly fibrillar, only 15 percent co-localized with collagen (Fig. 6c), and the non-collagen-colocalized population was physically separated from the collagen scaffold (Movies S9 and S10, ESI†). Thus the Fn fibrils assembled at these later time points are less stabilized by the collagen scaffold and more highly stretched by cell generated forces. The decrease in FRET observed for the small amount of collagen-colocalized Fn-DA present between 48 and 72 hours is harder to explain, but may be due to the presence of mechanically stretched Fn fibers that we are unable to spatially resolve from the collagen scaffold or due to the adsorption of Fn molecules to the collagen scaffold in a more mechanically unfolded conformation. These results reveal that in contrast to simplified 2D systems, many factors within a dynamic 3D collagen matrix will contribute to the molecular composition of the matrix subsequently assembled by cells.

To assess the incorporation and stability of plasma Fn in microtissues, we also investigated the relative fluorescence intensities of the labeled plasma Fn during these pulse experiments. Interestingly, the integrated intensity of the emission spectra of the Fn-DA (the sum of both the donor and acceptor fluorophores when exciting the donors) was dramatically lower for Fn-DA that was present from 0–24 hours in microtissues that were fixed after 72 hours of remodeling as compared to those that were fixed after 24 hours (Fig. S5, ESI†) indicating a degradation of the initial Fn-DA during tissue remodeling. Note that these values do not represent Fn conformation (which did not change between these two conditions), but rather the relative amounts of Fn-DA present in the microtissues. We also noticed that Fn-DA present in culture from 48–72 hours (in microtissues fixed after 72 hours) had dramatically lower integrated emission intensity than Fn-DA present from 0–24 hours in microtissues that were fixed after 24 hours (Fig. S5, ESI†). Because the Fn-DA in these two experiments was present in culture for the same amounts of time, it is unlikely that proteolytic degradation alone could explain the difference in integrated intensity, but rather that the decreased intensity of the 48–72 hours Fn-DA is also due to a dilution with unlabeled endogenous cell-secreted Fn in fibrils as confirmed by the colocalization of both exogenous plasma Fn and endogenous cellular Fn in the pericellular matrix (Fig. S3, ESI†).

Discussion

ECM assembly often involves the deposition of both provisional matrices such as Fn and more permanent matrices such as the collagens. During normal wound healing and in tissue culture, a type-I collagen matrix is deposited along and highly co-localized with Fn fibers.⁶ In collagen based surgical implants and in 3D *in vitro* cell culture, cells are frequently placed in the inverse scenario. Namely, cells are encapsulated into an initial collagen scaffold within which they then assemble their own ECM. By combining MEMS based μ TUGs with Fn FRET probes, we directly measured the spatial distributions and molecular conformation of Fn within 3D, collagen-based microtissues. We show that soluble and thus compact Fn from media quickly adsorbs to and is stabilized by the collagen scaffold, whereas fibrillar Fn was later assembled by cells predominantly at the tissue periphery. This new fibrillar ECM is a combination of cell-derived and plasma Fn, and becomes spatially segregated from the collagen fibers which are compacted at the tissue core. The net result of this process is that cells are increasingly isolated from the initial Fn coated collagen scaffold and progressively immersed in the new cell-assembled Fn-rich ECM that displays a rather different set of molecular conformations.

We found that the FRET signal from our Fn-DA probe progressively decreased as cells remodeled the collagen scaffold reflecting a transition from primarily compact to primarily stretched Fn molecules. The higher FRET signal seen from collagen-colocalized Fn (as compared to non-collagen-colocalized Fn) could be due to mechanical stabilization of the Fn fibers by the collagen scaffold, or due to residual non-fibrillar Fn present in our measurement volume. Importantly, these two distinct Fn populations (compact/adsorbed and extended/fibrillar) may have dramatically different signaling implications given the fact that Fn has multiple cryptic and mechano-regulated binding sites.²⁰ However, even when the microtissue was tethered to rigid boundaries, the relative loss in secondary structure (indicating exposure of cryptic sites) of Fn-DA assembled within microtissues is significantly less than what has been shown for Fn-DA assembled by cells cultured on rigid glass coverslips.¹² We hypothesize that this discrepancy may be due to the large presence of compact, collagen-adsorbed Fn molecules, the reduced rigidity of the collagen matrix (as compared to glass), or due to a portion of the mechanical load in 3D microtissues being distributed through the exogenous collagen scaffold instead of being transferred directly to Fn fibers.

Further, although cell generated forces promote the assembly of nascent Fn fibrils,¹¹ we found that 60% of the decrease in Fn-DA FRET signal that occurred during microtissue remodeling was not affected by acute treatment with blebbistatin. This signal likely represents the drop in FRET that occurs during the transition from a predominantly compact form of Fn adsorbed to the collagen scaffold to a predominantly fibrillar pericellular matrix. Once incorporated into fibrils, Fn-DA molecules display a lower FRET than those in solution and than those adsorbed to the collagen scaffold. This drop in FRET represents an irreversible transition and will not be affected by treatment with blebbistatin. However, the fibrillar Fn population also becomes progressively stretched by cell generated tractions²² resulting in further molecular extension and a drop in FRET signal.¹⁰ This traction-induced fiber

stretching likely represents the 40% of the FRET signal that was restored upon blebbistatin treatment.

In addition to stretching Fn fibers, cell-generated tractions also drive the long-term remodeling of the collagen scaffold. Indeed, this phenomenon has been studied extensively and several quantitative models now describe the relationship between collagen remodeling/alignment, cell tractions, and tissue geometry.²³ Importantly, while the collagen fibers within microtissues do not individually co-localize with fibrillar Fn (as is the case during normal wound healing), they collectively serve as a dynamic biomaterial substrate that governs overall tissue geometry and against which cells pull to assemble fibrillar Fn. For microtissues cultured while pinned to 2 flexible cantilevers, we found that Fn–DA FRET decreased concurrently with increases in tissue stress; however, we did not notice a clear correlation between microtissue stress and Fn molecular strains (measured *via* Fn–DA FRET) within each time point, indicating that the overall tissue stress and Fn molecular strains might not be directly related in this multi-component microtissue. Indeed, even in highly simplified systems, generating a constitutive relationship to relate tissue stress and matrix strain is complicated by the dynamic and complex mechanics of the collagen matrix.²⁴ Our studies highlight that although cells are initially encapsulated in a collagen scaffold, they quickly become immersed and ultimately reside within a Fn-rich cell-derived matrix. Understanding how tissue stresses and strains are related at cellular and sub-cellular length scales will thus require knowledge of not only the mechanics of each particular matrix type (*e.g.* collagen and Fn for this simplified example), but also of the nature and dynamics of how stresses and strains are partitioned between the various ECM components, which are differentially coupled *via* integrins to the actin cytoskeleton. Although this is a daunting prospect, 2D studies utilizing inert glass slides or polyacrylamide gels have found that (1) Fn matrix fibers are progressively extended and unfolded by cell generated forces;^{10,22} (2) Fn fibers assembled on rigid substrates are more unfolded than those assembled on soft polyacrylamide substrates,¹⁸ and (3) crosslinking of fibrillar Fn matrices increases their rigidity and prevents their unfolding.¹² These properties have recently been utilized for “material driven ECM assembly” to engineer the conformation of Fn on polymer scaffolds leading to increased myogenic differentiation of adhered cells.²⁵ However, collagen gels and many biomaterial implants are not inert substrates, but can actively be remodeled by cells and all of the above processes likely contribute to the conformation of the Fn matrix presented to the cells.

In vivo, the physical conformation of Fn has been shown to regulate morphogenetic movements,²⁶ and cryptic binding sites exposed in mechanically extended Fn fibrils can regulate cell adhesion and matrix assembly,^{10,12} increase the nonspecific binding of albumin and casein,¹⁴ and destroy N-terminal bacterial binding sites.¹³ Here, the gradients in Fn conformation in our microtissue system appeared to serve as an “extracellular memory” whereby the mechanical signals experienced by cells are dependent not only on the current stresses, but also on the history of previous ECM remodeling events that are reflected in accumulated molecular strains. In contrast to focal adhesions, which respond quickly and directly to mechanical stress,²⁷ the molecular conformation of the Fn matrix is modulated by both

the instantaneous cell tractions (in the form of fiber stretching) and the history of previous ECM remodeling events that are reflected in the transition from adsorbed/compact to extended/fibrillar Fn. This long-term remodeling could serve as an “extracellular memory” and result in long-term patterns that will continue to signal to cells at a significantly longer time scale than the transient fluctuations in cell traction forces. Given the importance of Fn conformation to a cellular function, understanding how these patterns emerge and are maintained will be critical for dissecting the interplay between long-range morphogenetic movements and local microenvironmental manipulation of cell phenotype. Our studies show that FRET based readouts of molecular conformation combined with μ TUGs provide one approach to quantify such relationships, and highlight a means to understand the complex interplay between cells and matrix in highly anisotropic microenvironmental niches.

Materials and methods

Device fabrication and microtissue seeding

Single layer and multilayer templates were created as described previously.¹⁷ SU-8 photoresist (Microchem) was spin coated onto silicon wafers. Multilayer SU-8 masters were created using successive spin coat and exposure steps. To generate substrates for microtissues, SU-8 masters were cast with a prepolymer of PDMS (sylgard 184; Dow-Corning). Before cell seeding, the PDMS templates were sterilized in 70% ethanol followed by UV irradiation for 15 minutes and treated with 0.5% Pluronic F127 (BASF) to reduce cell adhesion. Liquid neutralized collagen I from rat tail (BD biosciences) was then added to the substrates on ice and templates were degassed under vacuum. Additional collagen and cells were then added to the mold and the entire assembly was centrifuged to drive the cells into the micropatterned templates. Excess solution was removed by dewetting the surface of the substrate prior to incubating at 37 °C to induce collagen polymerization. Fn containing media was then added to each substrate. All constructs in this study were prepared using a final concentration of 1.75 mg ml⁻¹ collagen.

Calculation of cantilever spring constant and microtissue force/stress

Cantilever spring constants were calculated utilizing a capacitive MEMS force sensor mounted on a micromanipulator as described previously.²⁸ Images of the sensor tip and cantilever head were acquired during each test using an Olympus FV1000 confocal microscope with an air immersion 0.4 NA 10 \times objective. To account for local deformation of the PDMS material around the sensor, the spring constant of the MEMS sensor was calibrated against the side of the PDMS well which can be viewed as an elastic half space of the same material modulus as the PDMS cantilevers and was found to be 104 \pm 1.9 nN μ m⁻¹. This value was then used for the subsequent measurements of the force required for cantilever bending. For each measurement the sensor tip was placed 20 microns below the top of the post and the probe translated laterally against the outer edge of the cantilever using a custom written Lab

View (National Instruments) script. The probe base was displaced approximately 150 microns for each measurement. The displacement of the probe tip (and thus of the cantilever head) was calculated from the spring constant measured above and the reported sensor force and was verified visually during the deformation. 5 cantilevers were measured across a substrate and measurements were repeated for three different substrates. Cantilevers were found to have linear responses up to approximately 40 microns of deformation. As the majority of cantilever deformations observed in this paper were below 40 microns, this section was fit using a linear fit with a spring constant of $148 \pm 35 \text{ nN } \mu\text{m}^{-1}$ which was then used for calculation of microtissue forces. Only microtissues that were uniformly anchored to the tips of the cantilevers were included in the analysis. Microtissue stress was calculated by imaging the entire volume of the microtissue within a $30 \mu\text{m}$ wide strip (measured along the long axis of the tissue) at the tissue midpoint. The cross-sectional area of this region was then measured from the confocal z -stack data using custom written Matlab (The Mathworks) scripts.

Fibronectin isolation, fluorescent labeling and denaturation curves

Fn was isolated from human plasma (Zurcher Blutspendedienst SRK) by affinity chromatography as described previously.¹⁰ For cysteine (acceptor) labeling, unlabeled Fn was denatured in 4 M urea at a concentration of 1 g l^{-1} and incubated with 40-fold molar excess of Alexa Fluor 546-maleimide (Invitrogen) for 3 hours at room temperature. Cysteine labeled Fn was separated from free dye using by a size exclusion chromatography PD-10 column (Sephadex) equilibrated with PBS with 0.1 M NaHCO_3 [pH 8.5]. Cysteine labeled Fn was then incubated with 60-fold molar excess Alexa Fluor 488-succinimidyl ester for 3 hours at room temperature to label amines (donors) before separating Fn-donor/acceptor (Fn-DA) from free dye with a second PD-10 column equilibrated in PBS. Fn-DA was then diluted to 0.3 g l^{-1} in PBS, aliquoted and stored at $-80 \text{ }^\circ\text{C}$ until needed. A labeling ratio of 4 acceptors and ~ 7 donors per Fn dimer was determined by measuring the absorbances of Fn-DA at 280, 496 and 56 nm and using published extinction coefficients for dyes and Fn. Unlabeled Fn was isolated in a similar manner, dialyzed in PBS for 48 hours (Slide-a-lyzer dialysis cassette, 10 000 MW cutoff, Pierce) and diluted to 1 g l^{-1} in PBS before aliquoting and storing at $-80 \text{ }^\circ\text{C}$. Before use, Fn-DA or Fn was thawed on ice for 1 hour to avoid protein precipitation. After thawing, all samples were stored at $4 \text{ }^\circ\text{C}$ and used within 72 hours. All cell culture experiments utilized unlabeled Fn in 10-fold excess to Fn-DA in order to avoid signal from intermolecular FRET. Denaturation curves were obtained by diluting Fn-DA to a final concentration of 0.1 g l^{-1} in specified concentration of GdnHCl, and imaging with confocal microscopy under identical parameters to those used for cell culture.

Confocal microscopy

Z -stack images were acquired using an Olympus FV1000 confocal microscope with a water immersion 0.9 NA 40 \times objective. Four post microtissue images were acquired at 512×512 pixels per

slice with $2 \mu\text{m}$ slice spacing for voxel dimensions of $0.621 \times 0.621 \times 2.0 \mu\text{m}$. The mid-sections of 2 post microtissue images were acquired at 256×256 pixels with $1.5\times$ zoom factor per slice with $2 \mu\text{m}$ slice spacing for voxel dimensions of $0.828 \times 0.828 \times 2.0 \mu\text{m}$. All images were acquired with $3\times$ Kalman line averaging. FRET images were acquired using a single photo multiplier tube (PMT) by sequentially acquiring images through a diffraction grating and slit. Donor and acceptor intensities were detected using 20 nm bandwidths centered at 510–530 nm and 560–580 nm, respectively. Serial imaging of the same volume confirmed that no photo bleaching was occurring. To ensure that no artifacts occurred due to the microscope setup, laser power, pixel dwell time and PMT voltage were kept constant between all conditions (all experiments and all time points) for imaging protein and DNA densities and Fn-DA FRET. Images of fluorescent beads within microtissues were acquired on a Zeiss LSM 710 laser scanning confocal microscope with a water immersion 1.1 NA 40 \times objective.

FRET calculation and colocalization analysis

FRET ratios are reported as the intensity of the acceptor (I_a) divided by the intensity of the donor (I_d). All images were 12-bit (4096 relative intensity units) and were processed with custom written Matlab (The Mathworks) scripts. First, background values were determined from tissue-free regions of each image and subtracted from the raw images. Then, images of each channel were binary thresholded using a cutoff value of $2\times$ background (Fn donor and acceptor), $1.75\times$ background (collagen), and $1.5\times$ background (DAPI). These settings were determined empirically based on the intensity of each fluorescence signal and then kept constant for all experiments. Prior to calculation of the FRET ratio, donor and acceptor images were smoothed using a 2×2 pixel local averaging filter. Donor bleed through was calculated from images of microtissues labeled with Alexa-488 Fn and was determined to be a linear function of donor intensity with a slope of 0.224 (*i.e.* approximately 20% of the donor intensity was present in the acceptor channel). Acceptor images were thus scaled appropriately prior to calculation of the FRET ratio. Any saturated pixels, or those below the threshold value were excluded from the FRET analysis. Median values were calculated for each tissue from all pixels above threshold with a single tissue considered as an independent observation. Colocalization analysis was performed on a voxel by voxel basis with Fn considered to be colocalized with collagen if each channel was above the aforementioned threshold values. These imaging conditions, combined with the thin profile of the microtissues, were optimized to avoid any confounding contributions due to aberration from the collagen based microtissues. However, we wanted to further validate that imaging into the depth of the microtissue would not cause spectral artifacts and thus confound our FRET data. To this end, we incorporated $0.5 \mu\text{m}$ fluorescent beads (Invitrogen) within the microtissues and imaged their intensities as a function of tissue depth. Imaging through the collagen rich microtissues had no appreciable effect on either the integrated brightness nor the peak intensities of beads with emission peaks at either 486 or 605 nm (similar to the FRET probes used in the study) (Fig. S6, ESI[†]).

Immunofluorescent staining and protein density mapping

Microtissues were cultured for the indicated periods of time before fixation with 4% formaldehyde in PBS for 1 h at 37 °C. Samples were subsequently rinsed for 30 minutes in PBS, before blocking overnight in 10% donkey serum. The exogenous collagen scaffold was labeled using primary antibodies directed against type-I rat collagen (Chondrex) and detected using fluorophore conjugated, isotype-specific, anti-IgG antibodies (Jackson ImmunoResearch). The use of primary antibodies specific for rat-tail collagen ensures that we only examine the localization of the original collagen scaffold and not collagen assembled *de novo* by the constituent NIH 3T3 cells (which are from mice). Cell nuclei were counter stained with DAPI. Density maps of protein and DAPI labeling were created by averaging the immunofluorescent (or FRET labeled Fn) data from individual microtissues. Cell-derived Fn was imaged utilizing an antibody specific to the EDA splice domain.²⁹ Plasma Fn density within microtissues was measured by computing the sum of the donor and acceptor fluorophores for Fn-DA excited at the donor wavelength. Masks were generated in Adobe Photoshop labeling the positions of each cantilever and used to align and crop the z-stacks of each microtissue. Optical slices from each tissue (10 tissues total) were then averaged to quantify protein and cell distributions for each condition. Because microtissues displayed small variations in thickness and in the vertical position at which they were tethered to the pillars, protein density maps were normalized by the thickness of each microtissue prior to averaging (*i.e.* plotted from the uppermost to the lower most surface of the tissue at each x - y position). Volume renderings of microtissues were constructed from confocal image stacks using Fiji. Protein alignment was computed using principal component analysis of the image gradients from the confocal images as described previously.^{17,30} The image gradient vector can be expressed as $\begin{bmatrix} G_x(x,y) \\ G_y(x,y) \end{bmatrix} = \text{sign} \left(\frac{\partial I(x,y)}{\partial x} \right) \begin{bmatrix} \frac{\partial I(x,y)}{\partial x} \\ \frac{\partial I(x,y)}{\partial y} \end{bmatrix}^T$. Principal component analysis (PCA) computes a new orthogonal basis such that the variance of the projection on one axis is maximal while the variance of the projection on the orthogonal axis is minimal. This process is akin to finding the eigenvector decomposition of the autocovariance matrix $C = \begin{bmatrix} G_{xx} & G_{xy} \\ G_{yx} & G_{yy} \end{bmatrix}$. The principal eigenvector corresponds to the direction of fiber alignment. Alignment strength maps are computed from the eigenvalues as $\text{str} = \frac{\lambda_1 - \lambda_2}{\lambda_1 + \lambda_2}$. Highly aligned regions ($\text{str} \sim 1$) represent fibrillar regions with uniformly aligned fibers. Weakly aligned regions ($\text{str} \sim 0$) represent either fibrillar regions with heterogeneous orientations or non-fibrillar (diffuse) staining. x - y alignment and strength values were computed for each confocal slice separately. The alignment maps for each tissue were then averaged from all confocal slices. Final alignment maps represent the compiled average from 10 different microtissues. The integrated intensity and peak brightness of fluorescent beads within microtissues were computed utilizing code adapted from ref. 31.

Statistical analysis

Statistical analysis was performed in Matlab utilizing the Kruskal–Wallis one-way analysis of variance and Tukey's HSD (Honestly significant difference) tests to illustrate

significance. Because the tests involve multiple comparisons, all statistical analysis are included in table format as Tables S1–S3 (ESI[†]).

Cell culture and reagents

NIH 3T3 fibroblasts (American Type Culture Collection, ATCC) were cultured in 4.5 mg ml⁻¹ glucose containing DMEM + L-glutamine (Gibco) supplemented with 10% bovine serum (Biowest). Cells were maintained at 37 °C and 5% CO₂ for all experiments. When indicated, Fn was added to the cell culture media at a total concentration of 50 µg ml⁻¹ (5 µg ml⁻¹ Fn-DA and 45 µg ml⁻¹ unlabeled Fn). Blebbistatin (Sigma, 50 µM) treatment was performed for 2 hours at 37 °C and 5% CO₂ prior to fixation.

Abbreviations

3D	three-dimensional
ECM	extracellular matrix
Fn	fibronectin
2D	two-dimensional
FRET	Foerster Radius Energy Transfer
MEMS	micro-electro-mechanical
µTUGs	microfabricated tissue gauges
PDMS	poly-dimethylsiloxane
Fn-DA	Donor/Acceptor labeled FRET based biosensor of Fn conformation
GdnHCl	guanidine hydrochloride

Acknowledgements

The authors thank Prof. Dario Neri for the gift of the EDA specific Fn antibody, Enrico Klotzsch, Yang Zhang, John Saeger, and Ingmar Schoen for experimental assistance and helpful discussions and Michael Borochin for assistance in fabricating the µTUG substrates. This work was supported by the ERC Advanced grant (VV) and the ETH Zurich and the NIH (HL73305 and HL90747), and the Nano/Bio Interface Center and Center for Engineering Cells and Regeneration of the University of Pennsylvania. WRL acknowledges financial support from the National Science Foundation Graduate Research Fellowship and the Whitaker International Fellows and Scholars Program.

References

- 1 F. Grinnell and W. M. Petroll, Cell motility and mechanics in three-dimensional collagen matrices, *Annu. Rev. Cell Dev. Biol.*, 2010, **26**, 335–361; S. Nakagawa, P. Pawelek and F. Grinnell, Extracellular matrix organization modulates fibroblast growth and growth factor responsiveness, *Exp. Cell Res.*, 1989, **182**, 572–582; D. Stopak and A. K. Harris, Connective tissue morphogenesis by fibroblast traction. I. Tissue culture observations, *Dev. Biol. (Amsterdam, Neth.)*, 1982, **90**, 383–398; D. Stopak, N. K. Wessells and A. K. Harris, Morphogenetic rearrangement of injected collagen in developing chicken limb buds, *Proc. Natl. Acad. Sci. U. S. A.*, 1985, **82**, 2804–2808.
- 2 T. Eschenhagen, C. Fink, U. Remmers, H. Scholz, J. Wattchow, J. Weil, W. Zimmermann, H. H. Dohmen, H. Schafer, N. Bishopric, T. Wakatsuki and E. L. Elson, Three-dimensional reconstitution of embryonic cardiomyocytes in a collagen matrix: a new heart muscle model system, *FASEB J.*, 1997, **11**, 683–694; D. G. Wallace and J. Rosenblatt, Collagen gel systems for sustained

- delivery and tissue engineering, *Adv. Drug Delivery Rev.*, 2003, **55**, 1631–1649; W. H. Zimmermann, I. Melnychenko, G. Wasmeier, M. Didie, H. Naito, U. Nixdorff, A. Hess, L. Budinsky, K. Brune, B. Michaelis, S. Dhein, A. Schwoerer, H. Ehmke and T. Eschenhagen, Engineered heart tissue grafts improve systolic and diastolic function in infarcted rat hearts, *Nat. Med.*, 2006, **12**, 452–458.
- 3 Y. Adachi, T. Mio, K. Takigawa, I. Striz, D. J. Romberger, J. R. Spurzem and S. I. Rennard, Fibronectin production by cultured human lung fibroblasts in three-dimensional collagen gel culture, *In Vitro Cell. Dev. Biol.: Anim.*, 1998, **34**, 203–210.
 - 4 R. Chiquet-Ehrismann, M. Tannheimer, M. Koch, A. Brunner, J. Spring, D. Martin, S. Baumgartner and M. Chiquet, Tenascin-C expression by fibroblasts is elevated in stressed collagen gels, *J. Cell Biol.*, 1994, **127**, 2093–2101.
 - 5 E. A. Davenport and P. Nettlesheim, Type I collagen gel modulates extracellular matrix synthesis and deposition by tracheal epithelial cells, *Exp. Cell Res.*, 1996, **223**, 155–162.
 - 6 K. E. Kadler, A. Hill and E. G. Canty-Laird, Collagen fibrillogenesis: fibronectin, integrins, and minor collagens as organizers and nucleators, *Curr. Opin. Cell Biol.*, 2008, **20**, 495–501; K. S. Midwood, L. V. Williams and J. E. Schwarzbauer, Tissue repair and the dynamics of the extracellular matrix, *Int. J. Biochem. Cell Biol.*, 2004, **36**, 1031–1037.
 - 7 J. Sottile and D. C. Hocking, Fibronectin polymerization regulates the composition and stability of extracellular matrix fibrils and cell-matrix adhesions, *Mol. Biol. Cell*, 2002, **13**, 3546–3559; J. Sottile, F. Shi, I. Rublyevska, H. Y. Chiang, J. Lust and J. Chandler, Fibronectin-dependent collagen I deposition modulates the cell response to fibronectin, *Am. J. Physiol. Cell Physiol.*, 2007, **293**, C1934–C1946.
 - 8 B. J. Dzamba, K. R. Jakab, M. Marsden, M. A. Schwartz and D. W. DeSimone, Cadherin adhesion, tissue tension, and non-canonical Wnt signaling regulate fibronectin matrix organization, *Dev. Cell*, 2009, **16**, 421–432.
 - 9 C. A. Lemmon, C. S. Chen and L. H. Romer, Cell traction forces direct fibronectin matrix assembly, *Biophys. J.*, 2009, **96**, 729–738.
 - 10 M. L. Smith, D. Gourdon, W. C. Little, K. E. Kubow, R. A. Eguiluz, S. Luna-Morris and V. Vogel, Force-induced unfolding of fibronectin in the extracellular matrix of living cells, *PLoS Biol.*, 2007, **5**, e268.
 - 11 C. Zhong, M. Chrzanowska-Wodnicka, J. Brown, A. Shaub, A. M. Belkin and K. Burridge, Rho-mediated contractility exposes a cryptic site in fibronectin and induces fibronectin matrix assembly, *J. Cell Biol.*, 1998, **141**, 539–551.
 - 12 K. E. Kubow, E. Klotzsch, M. L. Smith, D. Gourdon, W. C. Little and V. Vogel, Crosslinking of cell-derived 3D scaffolds up-regulates the stretching and unfolding of new extracellular matrix assembled by reseeded cells, *Integr. Biol.*, 2009, **1**, 635–648.
 - 13 M. Chabria, S. Hertig, M. L. Smith and V. Vogel, Stretching fibronectin fibres disrupts binding of bacterial adhesins by physically destroying an epitope, *Nat. Commun.*, 2010, **1**, 135.
 - 14 W. C. Little, R. Schwartlander, M. L. Smith, D. Gourdon and V. Vogel, Stretched extracellular matrix proteins turn fouling and are functionally rescued by the chaperones albumin and casein, *Nano Lett.*, 2009, **9**, 4158–4167.
 - 15 G. Baneyx, L. Baugh and V. Vogel, Fibronectin extension and unfolding within cell matrix fibrils controlled by cytoskeletal tension, *Proc. Natl. Acad. Sci. U. S. A.*, 2002, **99**, 5139–5143.
 - 16 T. Boudou, W. R. Legant, A. Mu, M. A. Borochoin, N. Thavandiran, M. Radisic, P. W. Zandstra, J. A. Epstein, K. B. Margulies and C. S. Chen, A microfabricated platform to measure and manipulate the mechanics of engineered cardiac microtissues, *Tissue Eng., Part A*, 2012, **18**, 910–919.
 - 17 W. R. Legant, A. Pathak, M. T. Yang, V. S. Deshpande, R. M. McMeeking and C. S. Chen, Microfabricated tissue gauges to measure and manipulate forces from 3D microtissues, *Proc. Natl. Acad. Sci. U. S. A.*, 2009, **106**, 10097–10102.
 - 18 M. Antia, G. Baneyx, K. E. Kubow and V. Vogel, Fibronectin in aging extracellular matrix fibrils is progressively unfolded by cells and elicits an enhanced rigidity response, *Faraday Discuss.*, 2008, **139**, 229–249; discussion 309–325, 419–420.
 - 19 L. Baugh and V. Vogel, Structural changes of fibronectin adsorbed to model surfaces probed by fluorescence resonance energy transfer, *J. Biomed. Mater. Res., Part A*, 2004, **69**, 525–534.
 - 20 V. Vogel, Mechanotransduction involving multimodular proteins: converting force into biochemical signals, *Annu. Rev. Biophys. Biomol. Struct.*, 2006, **35**, 459–488.
 - 21 D. C. Hocking, J. Sottile and K. J. Langenbach, Stimulation of integrin-mediated cell contractility by fibronectin polymerization, *J. Biol. Chem.*, 2000, **275**, 10673–10682; Y. Liu, R. Yanai, Y. Lu, K. Kimura and T. Nishida, Promotion by fibronectin of collagen gel contraction mediated by human corneal fibroblasts, *Exp. Eye Res.*, 2006, **83**, 1196–1204.
 - 22 T. Ohashi, D. P. Kiehart and H. P. Erickson, Dynamics and elasticity of the fibronectin matrix in living cell culture visualized by fibronectin-green fluorescent protein, *Proc. Natl. Acad. Sci. U. S. A.*, 1999, **96**, 2153–2158.
 - 23 F. Baaijens, C. Bouten and N. Driessen, Modeling collagen remodeling, *J. Biomech.*, 2010, **43**, 166–175; V. H. Barocas and R. T. Tranquillo, An anisotropic biphasic theory of tissue-equivalent mechanics: the interplay among cell traction, fibrillar network deformation, fibril alignment, and cell contact guidance, *J. Biomech. Eng.*, 1997, **119**, 137–145; E. A. Sander, T. Stylianopoulos, R. T. Tranquillo and V. H. Barocas, Image-based multiscale modeling predicts tissue-level and network-level fiber reorganization in stretched cell-compacted collagen gels, *Proc. Natl. Acad. Sci. U. S. A.*, 2009, **106**, 17675–17680.
 - 24 A. D. Freed and T. C. Doehring, Elastic model for crimped collagen fibrils, *J. Biomech. Eng.*, 2005, **127**, 587–593.
 - 25 M. A. Lan, C. A. Gersbach, K. E. Michael, B. G. Keselowsky and A. J. Garcia, Myoblast proliferation and differentiation on fibronectin-coated self-assembled monolayers presenting different surface chemistries, *Biomaterials*, 2005, **26**, 4523–4531; M. Salmeron-Sanchez, P. Rico, D. Moratal, T. T. Lee, J. E. Schwarzbauer and A. J. Garcia, Role of material-driven fibronectin fibrillogenesis in cell differentiation, *Biomaterials*, 2011, **32**, 2099–2105.
 - 26 T. Rozario, B. Dzamba, G. F. Weber, L. A. Davidson and D. W. DeSimone, The physical state of fibronectin matrix differentially regulates morphogenetic movements *in vivo*, *Dev. Biol.*, 2009, **327**, 386–398.
 - 27 B. Geiger, J. P. Spatz and A. D. Bershadsky, Environmental sensing through focal adhesions, *Nat. Rev. Mol. Cell Biol.*, 2009, **10**, 21–33.
 - 28 E. Klotzsch, M. L. Smith, K. E. Kubow, S. Muntwyler, W. C. Little, F. Beyeler, D. Gourdon, B. J. Nelson and V. Vogel, Fibronectin forms the most extensible biological fibers displaying switchable force-exposed cryptic binding sites, *Proc. Natl. Acad. Sci. U. S. A.*, 2009, **106**, 18267–18272.
 - 29 A. Villa, E. Trachsel, M. Kaspar, C. Schliemann, R. Somavilla, J. N. Rybak, C. Rosli, L. Borsi and D. Neri, A high-affinity human monoclonal antibody specific to the alternatively spliced EDA domain of fibronectin efficiently targets tumor neo-vasculature *in vivo*, *Int. J. Cancer*, 2008, **122**, 2405–2413.
 - 30 A. M. Bazen and S. H. Gerez, Systematic Methods for the Computation of the Directional Fields and Singular Points of Fingerprints, *IEEE Trans. Pattern. Anal. Mach. Intell.*, 2002, **24**, 905–919.
 - 31 Y. Gao and M. L. Kilfoil, Accurate detection and complete tracking of large populations of features in three dimensions, *Opt. Express*, 2009, **17**, 4685–4704.